AUTOMATIC IMAGE REGISTRATION OF MULTI-ANGLE IMAGERY FOR CHRIS/PROBA

J. Ma *, J.C.-W. Chan , F. Canters

Cartography and GIS Research Group, Department of Geography, Vrije Universiteit Brussel, Pleinlaan 2, 1050 Brussels, Belgium (Jianglin.Ma, Cheung.Wai.Chan, Frank.Canters)@vub.ac.be)

KEY WORDS: CHRIS/Proba, Automatic Registration, SIFT, Normalized Cross-correlation, Thin Plate Spline

ABSTRACT:

Subpixel image registration is the key to successful multi-angle remote sensing image applications such as image fusion, superresolution and classification. However, multi-angle remote sensing images pose some difficulties for automatic image registration, namely, 1) precisely locating control points (CPs) is difficult as large view angle images are susceptible to resolution change and blurring; and 2) local geometric distortion caused by variations in platform stability makes rigid transform models such as the projective model unreliable. In this paper we propose a two-stage automatic registration scheme for multi-angle remote sensing imagery. In the first step, CPs are gathered via the scale invariant feature transform (SIFT). However, CPs collected by SIFT may be too few or unevenly distributed. Therefore, another CPs collecting procedure based on normalized cross-correlation follows. In order to eliminate outliers in the CPs a geometric constraint is utilized; after outlier elimination in order to get CPs of high accuracy for the estimation of the thin plate spline model, which is used to solve the local geometric distortion problem, a pre-fitting procedure is adopted. The methodology developed in this paper is applied to three Compact High Resolution Imaging Spectrometer onboard the Project for On-board Autonomy (CHRIS/Proba) images. Experimental results demonstrate the efficiency and accuracy of the proposed method.

1. INTRODUCTION

Many recently available remote sensing imaging systems are equipped with multi-angle functions for a better understanding of the earth's surface character. These include the Multispectral Thermal Imager (MTI), the Multi-angle Imaging Spectro-Radiometer (MISR), the Along Track Scanning Radiometers (ATSR-1, ATSR-2, AATSR), and the Compact High Resolution Imaging Spectrometer onboard the Project for On-board Autonomy (CHRIS/Proba). The number of captured images and view angles varies from platform to platform. For example, the MTI can capture two images at 0° and 50° in a single pass, and the AATSR can observe the same target at view zenith angles of 0° and 55°. However, MISR can produce image stacks for nine camera angles (+70°, +60°, +45.6°, + 26.1°, 0°, -26.1°, -45.6°, -60°, -70°) and CHRIS/Proba provides multiple observations of the same scene at five different angles (+55°, +36°, 0°, -36°, -55°). These functionalities open up new applications in the areas of change detection, image fusion for classification and thematic map production, resolution enhancement and so on (Chan 2008a, Chan 2008b). However, for any successful application, accurate registration of these multi-angle images is a prerequisite. Automatic registration in these cases faces two main challenges: 1) images captured at large view angles are susceptible to resolution change and blurring, which makes precisely locating control points (CPs) difficult; 2) local geometric distortion caused by variations in platform stability is serious, which makes rigid transform models such as the projective model unreliable. A manual registration approach is not impossible in situations where a large number of images need to be registered. Also the accuracy of the manual approach can not be consistent as it strongly depends on decisions made by the operator. Thus, there is a pressing need for automatic image registration methods for multi-angle imagery.

A typical registration method can be divided into four steps: 1) feature detection; 2) feature matching; 3) transform model estimation; and 4) image resampling (Zitova and Flusser, 2003). There are many registration approaches, but depending on whether feature detection (step 1) is involved, registration methods can broadly be classified into two categories: area-based and feature-based methods (Zitova and Flusser, 2003).

Generally speaking, area-based methods have higher accuracy than feature-based methods, and they are particularly well-suited for images acquired from the same sensor (Eastman et al., 2007). However, there are difficulties in applying area-based methods directly on multi-angle imagery. Geometric distortion is usually high for images acquired at high view angles, making it impossible to use a rigid transform model such as the affine or projective transform. A viable alternative is to use a non-rigid registration model by searching for an adequate number of quality CPs and then estimating the model's parameters. However, if these CPs are gathered by first defining a window in the input image and then searching for a window match in the reference image, we face the problem of having to deal with a very large searching space (in the reference image). In order to solve this problem usually a coarse-to-fine hierarchical strategy is adopted. The template first finds candidate locations in the reference image at a coarse resolution, which can be obtained by way of the pyramid approach; then the positional accuracy is gradually improved by moving up to finer resolutions. However, for multi-angle imagery such as CHRIS/Proba, this method is not applicable as the gray level similarity between multi-angle imagery is weak due to

* Corresponding author

resolution disparity and severe blurring. Comparatively, feature-based methods that work on image features are more robust to variations in view angle and are therefore more suited for multi-angle imagery registration (Capel and Zisserman, 2003). However their disadvantage is that the number of detected CPs is sometimes few and therefore will cause problems for the estimation of a complex non-rigid transform model such as the thin plate spline (TPS) or piecewise linear (PL) model. To tackle the above-mentioned problems, we outline in this paper an automatic registration method that integrates the merits of both area-based and feature-based methods. It involves a two-stage CPs detection scheme where candidate CPs are collected first with the scale invariant feature transform (SIFT) method and then with a template matching method using normalized cross-correlation (NCC) as a criterion. It also incorporates a hierarchical approach to refine the collected CPs. The outliers in the SIFT CPs are discarded by the ambiguity criterion and a robust estimation of the projective transform model with *m*-estimator sample consensus (MSAC) (Torr and Zisserman, 2000); the outliers in the NCC CPs are eliminated by a spatial constraint instead of a threshold on the NCC coefficients. In order to make sure CPs are as accurate as possible, a final iterative refining procedure based on the statistical nature of CPs is performed to remove CPs of low accuracy. The TPS model is finally estimated via the selected CPs. The non-rigid TPS model is adopted to surmount the serious local distortion problem in multi-angle imagery.

We tested our approach on three sets of CHRIS/Proba images and accurate registration results are attained. In the following section the methodology is described (section 2). Experimental results are presented in section 3. Section 4 focuses on major conclusions and directions for future research.

2. METHODOLOGY

The proposed registration method is composed of four stages (Figure. 1). Each stage is described in detail below.

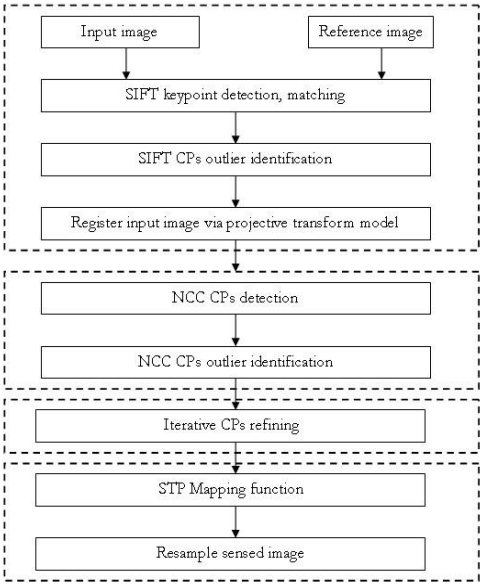

Figure 1. Flow chart showing the processing chain

2.1 SIFT Control Points Selection

Among various local feature detection methods, SIFT is a promising approach because it improves detection stability in situations of noisy input (Lowe, 2004). The method is also preferable when changes occur in scale, illumination, and to a certain extent in the 3D camera viewpoint. It achieves almost real-time performance and the detected features are highly distinctive. An extensive evaluation of various local descriptors' robustness in terms of viewing conditions and blurring effects is found in Mikolajczyk and Schmid (2005), and SIFT-based descriptors are described as the best performers. SIFT not only defines the position of detected points but also describes point detection quality. The detected SIFT points, also referred to as keypoints, are candidate CPs for feature matching. A keypoint descriptor is a quality measurement describing the region around the keypoint. The SIFT algorithm can be divided into four steps: scale-space extrema detection, keypoint localization, orientation assignment and keypoint descriptor assignment. As space is limited we refer the interested reader to Lowe (2004) for more details.

Once the keypoint descriptor has been calculated, keypoints can be matched by using the minimum distance method. However, not every pair of matched keypoints can be thought of as SIFT CPs as the keypoint descriptor only contains limited context and hence feature matching will often be ambiguous. Two criteria are used to filter out the outliers, or the bad pairs. The first criterion is T_{th}, an indicator of the ambiguity of each matched keypoint.

$$T_{th} = \frac{d_1}{d_2} \tag{1}$$

where d_1 is the distance to the nearest matched keypoint and d_2 is the distance to the second nearest. If T_{th} is close to 1, it means d_1 is close to d_2. That is to say, for a certain keypoint in the input image, SIFT detected two possible matching keypoints in the reference image. This is an ambiguous situation and the matched pair will be deleted if $T_{th} > 0.75$.

The second criterion is a spatial constraint based on the MSAC algorithm. Although local geometric distortion exists in multi-angle images, the main geometric relationship can still be represented by a projective transform model (Capel and Zisserman, 2003). MSAC utilizes this spatial relationship to eliminate falsely matched keypoints. MSAC, or *m*-estimator sample consensus, is an improved version of the RANDom Sample Consensus (RANSAC) algorithm, which has been widely used for rejecting outliers in matching points (Kim and Im, 2003). Both algorithms first estimate a projective model with four randomly selected points. After that the transform model is evaluated with regard to a fitting cost function:

$$C = \sum_i \rho(e_i^2) \tag{2}$$

where i refers to the ith matched keypoint pair and ρ is the error term defined as:

$$\rho(e_i^2) = \begin{cases} L & if \quad e_i^2 < T_m \\ T_m & if \quad e_i^2 \geq T_m \end{cases} \tag{3}$$

In equation (3) T_m is the threshold beyond which the matched keypoint pairs are considered outliers for the transform model, and $e_i^2 = (x_i - \underline{x_i})^2 + (y_i - \underline{y_i})^2 + (x_i' - \underline{x_i'})^2 + (y_i' - \underline{y_i'})^2$ is defined as the observed error function for a matched keypoint pair $(x_i, y_i) \leftrightarrow (x_i', y_i')$, with $(\underline{x_i}, \underline{y_i})$, $(\underline{x_i'}, \underline{y_i'})$ point positions calculated via the estimated projective transform model. L is a variable that determines the difference between RANSAC and MSAC. For RANSAC L=0, which means every inlier has the same effect on the estimated transform model; for MSAC $L = e^2$, which means every inlier has a different influence on the fitting of the estimated transform model. Thus, it permits more flexibility in setting T_m. In case T_m is set too high some outliers can be regarded as inliers. MSAC mitigates this by treating all inliers differently. The default setting for T_m is 64. In this study, the above procedures were repeated 500 times and the transform model with the lowest fitting cost function value C was selected. Finally, the projective transform is re-estimated using all the keypoint pairs whose observed error function e^2 values are lower than T_m. These keypoint pairs constitute the first set of CPs, which are referred to as SIFT CPs in the paper.

2.2 NCC Control Points Selection

The problem of using only feature-based SIFT to generate CPs is that the number of CPs may be too small and CPs may be unevenly distributed. To remediate this problem, an area-based CP selection procedure is initiated. First, an intermediate registered image is generated by applying the projective transform described in Stage 1. We will call this image the 'intermediate input image' and use it for a template matching procedure. The intermediate input image is separated into image chips of 64×64 pixels, and each chip is matched with a corresponding chip in the reference image via NCC, or normalized cross-correlation. The matched center points of the chip pairs are then used as candidate CPs. This way the number of CPs for the final non-rigid transform model estimation is increased. The NCC coefficient r is calculated as:

$$r = \frac{\sum_{i=1}^{R}\sum_{j=1}^{C}\left(g_T(i,j) - \overline{g}_T\right)\left(g_S(i,j) - \overline{g}_S\right))}{\left(\sum_{i=1}^{R}\sum_{j=1}^{C}\left(g_T(i,j) - \overline{g}_T\right)^2\left(g_S(i,j) - \overline{g}_S\right)^2)\right)^{1/2}} \tag{4}$$

where $g_T(i,j)$ and $g_S(i,j)$ represent the grey values of the image chips in the input image and in the reference image respectively. $\overline{g}_T$ and $\overline{g}_S$ are the corresponding mean grey values respectively. R and C are the numbers of rows and columns of the image chips.

NCC has the following advantages that make it well-suited for CP searching: 1) the NCC coefficient is brightness invariant, that is to say, in the case of changes in external illumination the NCC coefficient will not change. This is especially important for multi-angle imagery as objects captured at different view angles may have different illumination and reflectance characteristics; 2) NCC CPs are robust to blurring. While the NCC coefficient will vary with the blurring of the template, the position of its maxima will not change. This is also important for images acquired at high view angles as these usually suffer from serious blurring; 3) NCC is comparatively fast to calculate (Lewis, 1995); and 4) NCC CPs obtained from image chips will be evenly distributed across the whole image.

There are three important issues with regard to collecting NCC CPs. The first has to do with template size. The larger the template is, the more unique the matching entity will be. However, the calculation load will increase as well. In our implementation the template window size was set at 64×64 as a compromise between calculation load and accuracy. In most cases, this window size enables us to find enough salient image features like lines and ridges. The second issue is related to the size of the searching space. We define a searching space which is about one and a half times the size of the template in the intermediate input image, that means the searching space has a size of 96×96. As the intermediate input image almost overlaps with the reference image, such a large space can make sure the template can find the matching chip within the constrained space. The last issue is about how to arrive at subpixel accuracies. In many applications, such as superresolution image reconstruction, subpixel accuracy is required. However, NCC can only determine an integer value for the CP position. In order to obtain subpixel accuracy, a 2nd order polynomial around the position of the NCC coefficient maximum is established. Nine points are used to determine the 2nd order polynomial applying the least-squares method. The CP position with sub-pixel accuracy corresponds to the location where partial differentiation of the polynomial reaches a zero value.

After NCC CPs have been gathered, they need to be screened for outliers. Homogeneous areas such as sand and water, which show repetitive patterns or low contrast may lead to false matches. NCC may also fail when moving objects such as clouds and shadows occur in the imagery. The traditional way to eliminate outliers in NCC CPs is by thresholding the NCC coefficients. However, initial experiments showed that this method is not effective. It is difficult to define a proper threshold for all the images, and it often occurs that the matching is successful in spite of coefficient values smaller than the threshold, and vice versa. We therefore use a geometric constraint to detect outliers in NCC CPs. If the distance between a pair of CPs is larger than a threshold value T_d, it is regarded as an outlier. The default setting for T_d is 16.

2.3 Control Points Refining

At this stage in the process two groups of CPs have been obtained: one SIFT and one NCC set. Both sets have gone

through outlier detection procedures, and together they constitute the potential set of CPs for TPS model estimation. As TPS is based on interpolation, it is important to make sure that each pair of CPs is as accurate as possible.

At this stage, the objective is to obtain the most accurate CPs possible by pruning points with large random errors. This can be done by utilizing the statistical characteristics of the CPs. Given a true, noise-free CP $(\underline{x}, \underline{y})$ in the reference image, the probability density of the corresponding observed CP location (x, y) can be thought of as a normal distribution (Capel and Zisserman, 2003):

$$\Pr((x,y) \mid (\underline{x},\underline{y})) = \frac{1}{2\pi\sigma^2}\exp\left(\frac{(x-\underline{x})^2+(y-\underline{y})^2}{2\sigma^2}\right) \qquad (5)$$

The observed noisy point (x, y) is the detected CP in the reference image, and the true, noise-free point (x, y) comes from the calculated CP via the CP in the input image and an estimated 3rd polynomial transform model. The polynomial transform of the 3rd order has often been used when geometrical distortion is substantial, and the residual stochastic characteristics of the 3rd order polynomial transform have been well studied (Buiten and van Putten, 1997). While it is not the recommended transform model for multi-angle imagery, it has the following characteristics which make it suitable for pre-fitting: 1) the polynomial function is an approximation function, which means that a CP pair with a comparatively large random error will not dramatically degrade the polynomial function parameter estimation; 2) the approximately evenly distributed NCC CPs contribute to an unbiased estimation of parameters. For a normal distribution, about 99.7% of the values are within plus and minus three standard deviations from the mean. Therefore, if the measured error of a CP pair is larger than three standard deviations, it is considered as a large random error and the CP pair will be discarded.

The CPs refining stage can be summarized as follows:
(i) Define a 3rd polynomial transform model using the least-squares method with all the CPs.
(ii) Calculate the noise-free point position, and obtain the model residual *dx* and *dy* in the horizontal and vertical direction. Compute the mean and standard deviation of *dx* and *dy*, and eliminate the points whose *dx* or *dy* value is beyond three standard deviations.
(iii) Repeat the above procedures until the following condition is fulfilled: the residuals in both directions are within three standard derivations.

2.4 Image Warping

TPS is an interpolation function with the CPs having a one-to-one mapping relationship. TPS is also the only spline model that can be cleanly decomposed into a global affine and a local non-affine warping component, and thus it can account for the local deformation caused by optical effects, relief change and so on (Chui, 2000). The thin-plate spline interpolation function can be expressed as:

$$\begin{pmatrix} f(x,y) \\ g(x,y) \end{pmatrix} = \begin{pmatrix} h_{11} & h_{12} \\ h_{21} & h_{22} \end{pmatrix}\begin{pmatrix} x \\ y \end{pmatrix} + \begin{pmatrix} h_{13} \\ h_{23} \end{pmatrix} + \begin{pmatrix} \sum_{i=1}^{N} F_i r_i^2 Inr_i^2 \\ \sum_{i=1}^{N} G_i r_i^2 Inr_i^2 \end{pmatrix} = \begin{pmatrix} x' \\ y' \end{pmatrix} \qquad (6)$$

where (x, y) is the coordinate in the input image, and $(f(x, y), g(x, y))$ is the coordinate in the reference image. (x_i, y_i) is the detected CP position in the input image. $r_i^2 = (x-x_i)^2 + (y-y_i)^2$ represents the distance between (x, y) and (x_i, y_i), and $h_{11},...,h_{23}$ define an affine transform matrix. F_i and G_i are the weights of the non-linear radial interpolation function.

To solve equation (6) with N pairs of CPs, the following equilibrium constraints are imposed:

$$\begin{cases} \sum_{i=1}^{N} F_i = \sum_{i=1}^{N} F_i x_i = \sum_{i=1}^{N} F_i y_i = 0 \\ \sum_{i=1}^{N} G_i = \sum_{i=1}^{N} G_i x_i = \sum_{i=1}^{N} G_i y_i = 0 \end{cases} \qquad (7)$$

With N pairs of CPs and the six equations in equation (7), we can solve the $2N+6$ unknown parameters in the TPS model. A more compact calculation for the unknown parameters is expressed as:

$$\begin{bmatrix} 0 & 0 & 0 & 1 & 1 & ... & 1 \\ 0 & 0 & 0 & u_1 & u_2 & ... & u_n \\ 0 & 0 & 0 & v_1 & v_2 & ... & v_n \\ 1 & u_1 & v_1 & 0 & r_{12}^2 Inr_{12} & ... & r_{1n}^2 Inr_{1n} \\ 1 & u_2 & v_2 & r_{21}^2 Inr_{21} & 0 & ... & r_{2n}^2 Inr_{2n} \\ ... & ... & ... & ... & ... & ... & ... \\ 1 & u_n & v_n & r_{n1}^2 Inr_{n1} & r_{n2}^2 Inr_{n2} & ... & 0 \end{bmatrix}\begin{bmatrix} h_{13} & h_{23} \\ h_{11} & h_{21} \\ h_{12} & h_{22} \\ F_1 & G_1 \\ F_2 & G_2 \\ ... & ... \\ F_n & G_n \end{bmatrix} = \begin{bmatrix} 0 & 0 \\ 0 & 0 \\ 0 & 0 \\ x_1 & y_1 \\ x_2 & y_2 \\ ... & ... \\ x_n & y_n \end{bmatrix} \qquad (8)$$

After the parameters of the TPS model have been estimated, the warping of the input image can be performed using the TPS model and the bilinear resampling function.

3. EXPERIMENTS

The proposed method was tested on multi-angle CHRIS/Proba imagery. All the images were acquired in mode 3 at five different view angles. The result of the 18th band (1002 - 1035 nm) will be used as a demonstrator. The reference image is the nadir image. Details of the data sets are described in Table I.

Site	Country	Time
Kalmthout	Belgium	1st July, 2008
Dijle Valley	Belgium	20th May, 2008
Ginkelse Heide	TheNetherlands	22nd Oct., 2007

Table 1. Study area

The pre-processing of CHRIS/Proba was done with the open-source software BEAM CHRIS-Box. It includes two important procedures: 1) noise reduction: replace missing data and de-striping; 2) atmospheric correction: retrieve the surface reflectance from remotely sensed imagery by removing the atmospheric effect (Guanter, 2005).

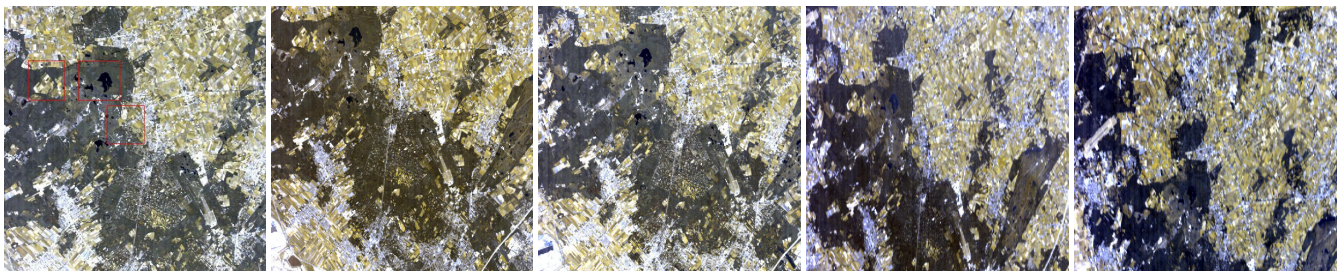

(a) (b) (c) (d) (e)

Figure 1. Multi-angle CHRIS/Proba imagery for the Kalmthout site: (a) Nadir (the squares correspond to the zones shown in detail in Figure 2), (b) +36°, (c) -36°, (d) +55°, (e) -55°.

Figure 1 shows the 18th band for the five multi-angle images (+/-55°, +/-36°, and 0°) for the Kalmthout site. It is clear from Figure 1 that blurring for large view angles (+/- 55°) is serious and that illumination conditions vary with different view angles. All the off-nadir images were co-registered to the nadir image using the proposed method.

Twenty sets of manually selected CPs were used as ground truth. The registration accuracy, represented by the root mean square error (RMSE), was calculated for each registered image as shown in Table 2.

Site	Angle	RMSE
Kalmthout	+36	0.1266
	-36	0.1492
	+55	0.1526
	-55	0.1655
Dijle Valley	+36	0.1239
	-36	0.1114
	+55	0.2124
	-55	0.1335
Ginkelse Heide	+36	0.1271
	-36	0.1211
	+55	0.3506
	-55	0.2991
Average	-	0.1727

Table 2. Registration accuracy for different images

The average registration accuracy assessed by means of a set of manually selected CPs is about 0.1727 pixels, which is very high. The results also show that on average the registration error for larger view angles at +/-55° is higher than for smaller view angles at +/-36°, which is normal. Results of visual evaluation of the proposed algorithm are shown in Figure 2. Three zooms are provided showing that the registered image fits well with the reference image across the whole scene.

4. CONCLUSION

In this paper a two-stage registration scheme is proposed. Salient SIFT CPs are detected first and then used for the estimation of the projective transform in stage 1. SIFT is shown to be a good feature detection method for multi-angle imagery. Even in the case of severe blurring and large resolution disparity between multi-angle imagery, at least 4 pairs of true SIFT CPs can be detected for the intermediate projective transform model estimation. The outliers in the set of candidate SIFT CPs can be successfully identified via the ambiguity identifying true SIFT CPs but also vital for detecting subsequent NCC CPs. Our experiments also testify that without this outlier procedure the intermediate input image will not overlap well with the reference image, which will make subsequent NCC CP detection fail.

NCC has also been proven to be a good area-based CP detection method for obtaining evenly distributed CPs in stage 2. After pre-registration the intermediate input image has geometric characteristics similar to the reference image. This intermediate step not only makes template matching much easier because the searching space is more constrained but also makes the NCC matching criterion hold. For example, if two image chips are of a different spatial resolution, which is the case for multi-angle imagery, NCC will fail. Also NCC's robustness to illumination change and blurring makes it particularly suited for CP detection, starting from the intermediate input image.

The iterative CP refining procedure in stage 3 is based on two assumptions: (1) the density of observed CPs is Gaussian, and (2) a 3rd order polynomial function is an empirically more appropriate global transform model for multi-angle imagery. Actually before the automatic registration method for CHRIS/Proba was proposed, different transform models were tested with CPs selected by hand. The 3rd order polynomial model proved to be a better transform model than other global transform models. During the refining procedure bad CPs with large random errors are successfully identified, however, a small part of the good CPs with high accuracy are eliminated as well. Indeed, while the 3rd order polynomial model residual can be thought of as an indictor of a bad pair of CPs, the large model residual can not guarantee it really is (Buiten and Van Putten, 1997). Visual inspection of the final CPs demonstrates that after CP refining only CPs with high accuracy are left.

The TPS model in stage 4 not only helps to deal with local distortion in multi-angle imagery but also helps to reach sub-pixel registration accuracy. Another key component to reach sub-pixel accuracy is that the CPs themselves are detected with sub-pixel accuracy by way of interpolation.

The overall results obtained with three multi-angle CHRIS/Proba image sets are encouraging. The proposed

method can also be applied on other multi-angle imagery from systems such as MTI and MISR.

ACKNOWLEDGEMENTS

The authors would like to express their grateful thanks to Luis Guanter who helped to generate the reflectance images used in this study. The research presented in this paper is funded by the Belgian Science Policy Office (BELSPO) in the frame of the STEREO II programme - project HABISTAT (SR/00/103).

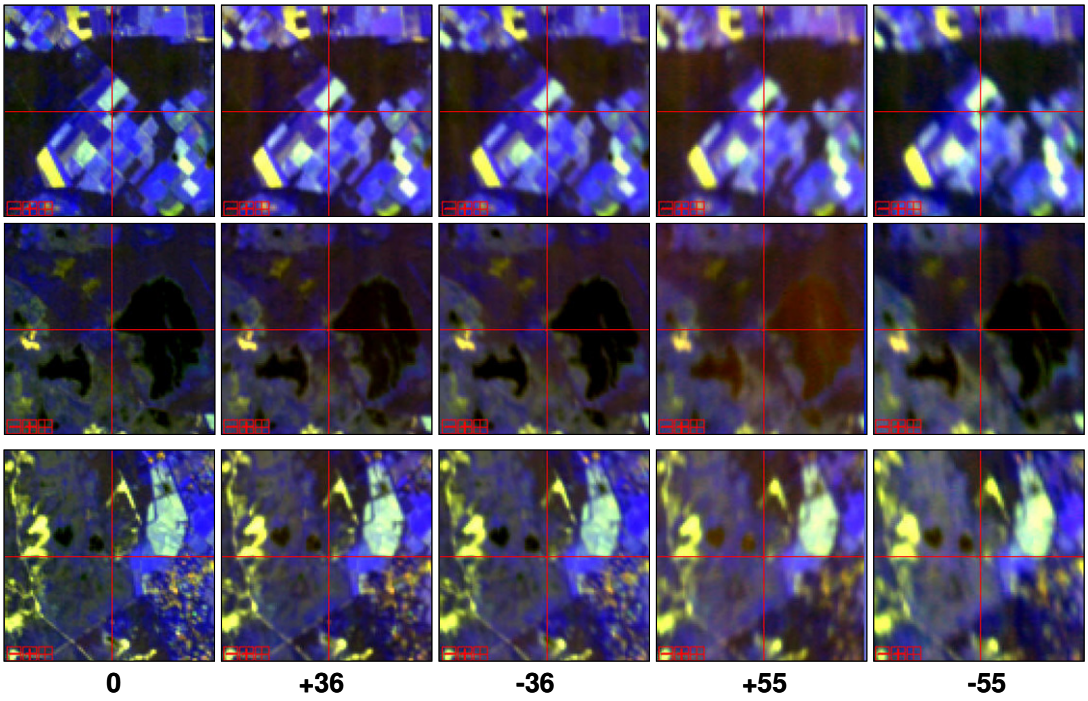

Figure 2. Registration results for the Kalmthout site. The first, second and third row correspond to the upper left corner, the center and the bottom right corner of Figure 1 respectively. In each row the centers of the cross correspond to the same point at different view angles after registration.

REFERENCES

Buiten, H.J. and van Putten, B., 1997. Quality assessment of remote sensing image registration – analysis and testing of control point residuals. *ISPRS Journal of Photogrammetry and Remote Sensing*, vol. 52, pp. 57-73.

Capel, D., and Zisserman, A., 2003. A Computer vision applied to super resolution. *IEEE Signal Process.*, 20(3), pp. 75-86.

Chan, J.C.-W., Ma, J. and Canters, F., 2008a. A comparison of superresolution reconstruction methods for multi-angle Chris/Proba images. *Proceedings of SPIE Image and Signal Processing of Remote Sensing XIV*, pp 1-11.

Chan, J.C.-W., Ma, J., Kempeneers, P., Canters, F., Vandenborre, J. and Paelinckx, D., 2008b. An evaluation of ecotope classification using superresolution images derived from Chris/Proba data. *Proceedings of IGARSS*, Vol. III, pp 322-325.

Chui, H. and Rangarajan, A., 2000. A new algorithm for non-rigid point matching. *IEEE Conference on Computer Vision and Pattern Recognition (CVPR),* vol. 2, pp. 44-51.

Eastman, R.D, Moigne, J.L, Netanyahu, N.S., 2007. Research issues in image registration for remote sensing. *IEEE Conference on Computer Vision and Pattern Recognition*, 2007, pp. 1-8.

Guanter, L., Alonso, L. and Moreno, J., 2005. A method for the surface reflectance retrieval from PROBA/CHRIS data over land: application to ESA SPARC campaigns. *IEEE Trans. Geosci. and Remote Sensing*, 43(12), pp. 2908-2917.

Kim, T. and Im, Y.J., 2003. Automatic satellite image registration by combination of matching and random sample consensus. *IEEE Trans.Geosci. and Remote Sensing,* 41(5), pp. 1111-1117.

Lewis, J.P., 1995. Fast template matching. *Proc. Vision Interface,* pp.120-123.

Lowe, D.G., 2004. Distinctive image features from scale-invariant keypoints. *International Journal of Computer Vision,* 60(2), pp. 91-110.

Mikolajczyk, K. and Schmid, C., 2005. A performance evaluation of local descriptors. *IEEE Trans. Pattern Anal. Mach. Intell.*, 27(10), pp. 1615-1630.

Torr, P.H.S. and Zisserman, A., 2000. MLESAC: A new robust estimator with application to estimating image geometry. *Computer Vision and Image Understanding*, 78(1), pp.138-156.

Zitova, B and Flusser, J, 2003. Image registration methods: a survey. *Image and Vision Computing,* 21(11). pp. 977-1000.